View metadata, citation and similar papers at core.ac.uk
brought to you by CORE
provided by Crossref

JMEPEG (2013) 22:2366–2376
DOI: 10.1007/s11665-013-0516-0
©The Author(s). This article is published with open access at Springerlink.com
1059-9495/$19.00

Optical Interference During rf-GDOES Depth Profiling of Anodized Aluminum-Tantalum Alloy Films

D. Ifezue

(Submitted December 29, 2012; in revised form January 21, 2013; published online March 19, 2013)

The optical interference effect observed in radio frequency glow discharge optical emission spectroscopy (rf-GDOES) depth profiles of anodic oxide films formed on several aluminum-tantalum alloys is investigated and then used to determine refractive index, thickness, and composition of the anodized Ta-Al alloy layer. Refractive indices at the tantalum wavelength (1.4-2.4) were found to increase approximately linearly with the Ta_2O_5/Al_2O_3 ratio in the inner layer of the anodic oxide film. The optical interference effect was used to determine the composition of the inner film layer from the intensity/time rf-GDOES depth profile with excellent agreement with RBS-derived values. Good accuracy is obtained for constant sputtering rates and hence good interfacial depth resolution and for intensity signals oscillating uniformly across the film. A procedure is also proposed for calculating the thickness of the transparent layer of the anodic oxide film using the refractive index value derived from calibration plots of refractive index versus Ta_2O_5/Al_2O_3 ratio. The quantified depth profile of anodized Ta-24at.%Al alloy is presented. There is excellent accuracy of the quantified composition. The accuracy of the film depth, however, has a strong correlation with calculated density.

Keywords aluminum, coatings, electronic materials

1. Introduction

Typical transmission electron micrographs of anodic oxide films formed on Ta-Al alloys reveal a thin outer alumina layer and an inner layer composed of units of Ta_2O_5 and Al_2O_3. Corresponding rf-GDOES depth profiles show oscillation of the tantalum and aluminum intensity signals, which is attributed to double reflection of the light emission incident on the film surface during sputtering. Thus, one portion of the light emission is reflected from the specimen surface, while the remaining portion traverses through the sample thickness and is subsequently reflected from the film/alloy interface. Both reflected lights interfere, and the changing sample surface results in the observed modulation of the intensity signal with depth. Similar effects have also been observed during rf-GDOES depth profiling of borophosphosilicate glass (BPSG), SiO_2, TiO_2, and $BaTiO_3$ on silicon substrates (Ref 1-3) (Fig. 1). Specifically, the optical interference effect on anodic oxide films formed on Ta-Al alloys is generally observed for films the thickness of which is a tiny fraction of the wavelengths of Tantalum and Aluminum. These films may therefore be of specific interest in building nanostructures (Ref 4).

Tantalum pentoxide (Ta_2O_5) has a wide range of practical applications which are based on its unique electronic and optical properties. The high refractive index (~2.23 nm at 363 nm) allows it to be used for fabrication of the glass for many photographic lenses (Ref 5). Between 300 nm and 2.0 μm, it is practically non-absorbent (i.e., colorless), which is the basis for a wide range of optical coatings (in the near-UV to IR spectra regions) such as anti-reflective coating for solar cells and charge coupled devices, light waveguides, birefringent coating, and as a component of multilayer interference filters (Ref 5, 6). The high dielectric constant ($\varepsilon \sim 25$) permits its use as capacitors in integrated circuits (Ref 7). Strong interest has also developed in using it as a capacitor material in low-inductance decoupling capacitors and in random access memories (Ref 5, 6, 8). It is chemically inert making it a good corrosion-resistant protective coating, and the barrier anodic oxide film can provide a blocking barrier (Ref 6). Ta_2O_5 is used in a wide range of microelectronic applications because of its long-term stability and low thermal coefficient of resistance (Ref 9-11)—it can only break down at >1470 °C (Ref 5). Ta-Al alloy films show improved temperature stability (temperature coefficient of resistance from +100 to −100 ppm degree/K) as the Ta contents of the alloy films increase from 7 to 15 at.% (Ref 4). Ta_2O_5 is used specifically in telecommunications, cell phones, laptop computers, pagers, and thin-film components. Interference effects during electroluminescence are reported for anodic films formed on aluminum (Ref 12) and on multiple-layer films including Ta_2O_5 (Ref 13) which has a wide enough bandwidth ($E_g \sim 4.2$ eV) to allow the exit of light. This effect has been used to determine the anodizing rate, film thickness (Ref 14), and refractive index of anodic alumina and optical constants of aluminum (Ref 12, 15). The optical effects of anodic alumina films are also the consequence of its high refractive index and low absorption. It exhibits double refraction in a transparent anisotropic medium (Ref 16). The observed interference effect for anodic alumina films has been used to calculate film thickness and refractive index (1.88 at 200 nm to 1.65 at 1300 nm) (Ref 14). Several other workers have also accurately measured the thickness of transparent oxide thin films using the method of light interference (Ref 17-19),

D. Ifezue, Wood Group Integrity Management, Staines TW18 1DT, UK. Contact e-mail: difezue@msn.com.

measuring the optical and electric properties where the refractive index and extinction coefficient were unknown (Ref 20). The measured thickness agreed well with values obtained by alternative methods. Chiu et al. (Ref 21) measured the thicknesses of anodic alumina films using cross-sectional TEM and then evaluated the data by ellipsometry to determine the refractive indices (1.48-1.67 as film thickness is increased from 70 to 133 nm). The error in the calculated refractive index is 0.01 for an extinction index of 0.002; therefore, they calculated their refractive index on the assumption that anodic alumina films were non-absorbing. They also found that thicker anodic oxide films exhibited comparable refractive indices to e-beam evaporated oxide films, but thinner anodic films have lower refractive indices than the evaporated films. The variation in refractive index was attributed to changes in stoichiometry and density. Van Gils (Ref 22, 23) proposed a method for quantifying the composition of anodic films formed on aluminum using infrared spectroscopic ellipsometry (IRSE) and supplemented by visible spectroscopic ellipsometry (VISSE).

This study discusses the interference effects observed in rf-GDOES depth profiles of several anodized Al-Ta alloys and subsequently used to determine film thickness, composition, and refractive index. Possible beneficial applications include optical coatings and devices which exploit the high refractive indices and interference effects of Ta and Al and for updating current rf-GDOES quantification software to include a feature which would permit transformation of qualitative intensity versus time depth profiles into composition versus depth (quantitative).

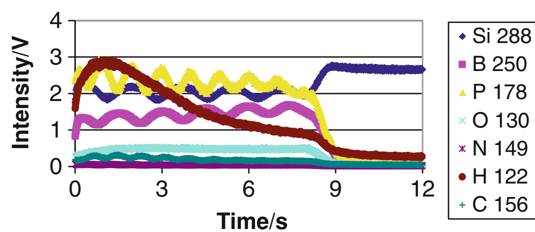

Fig. 1 Optical interference observed in the intensity/time rf-GDOES profile of a silicon wafer material used in production of hard disk memories (Ref 25)

2. Experimental

Seven Ta-Al alloys were prepared by deposition from separate targets (99.99% Al and 99.99% Ta) onto electropolished and anodized superpure aluminum in a magnetron sputtering system (Atom Tech. Ltd.). The chamber was first evacuated to 5×10^{-7} mbar and subsequently increased to 5×10^{-3} mbar when argon gas (99.99%) was introduced. The desired alloy composition was obtained by selecting a specific current value for each target. The deposition rate of the alloy is 0.45 nm s^{-1} and the final thickness attained is about 500 nm. The thickness deposited per revolution is 1.5 nm. The maximum temperature attained during sputter deposition is 35 °C. The Ta-Al alloys were then anodized at 5 mA/cm^2 and to 250 V in ammonium pentaborate solution. Anodizing was performed in the constant current or galvanostatic mode with the current preset at the desired value and the voltage free to find its own level from zero to the maximum value of the power supply. The voltage/time transients were monitored and recorded by means of PICOLOG for windows, release 5.03.4. The power supply unit (METRONIX 6911 DC) is capable of providing constant direct current up to 100 mA with an accuracy of $\pm$0.01%. Relatively large specimens with defined working are required for rf-GDOES analysis due to the large burn area required by the 4-mm anode size and the increased outer diameter defined by the size of the O-ring. After anodizing, the specimen was removed rapidly from the cell, washed thoroughly in distilled water, and then dried in a stream of cold air. The specimen was then stored in a desiccator until required for further examination. Thin strips from each anodized sample were prepared for ultramicrotomy (by means of the LEICA ULTRACUT ultramicrotome). Subsequently, a JEOL FX 2000 II transmission electron microscope, operating at 120 KV, was employed to examine the ultramicrotomed cross sections. The intensity/time qualitative depth profile of each film was obtained by rf-GDOES, with sputtering at an optimized power and pressure of 40 W and 600 Pa, respectively, corresponding to the highest depth resolution. A 13.56 MHz radio frequency generator was used to excite a luminescent discharge. The Jobin Yvon GD Profiler instrument was used for the analysis. For validation purposes, compositional depth profiling analysis was also undertaken by Rutherford Backscattering Spectroscopy

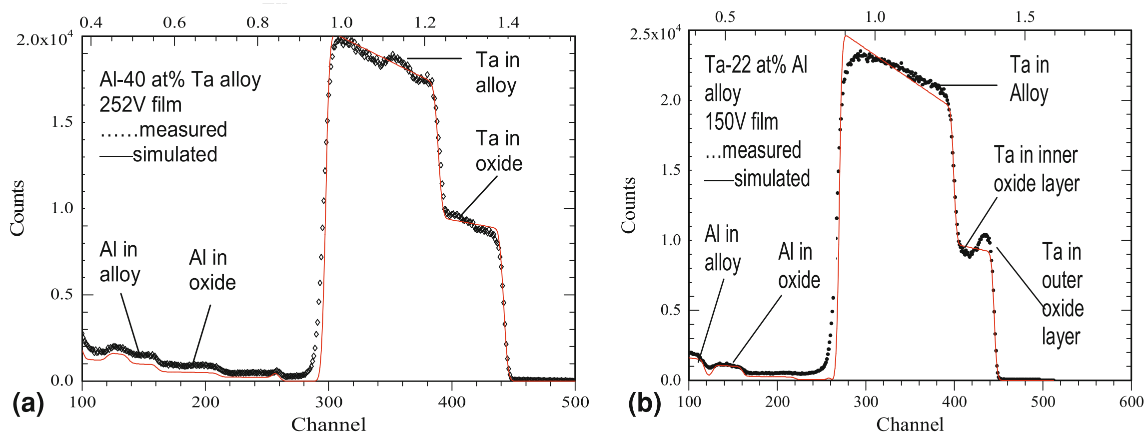

Fig. 2 Measured and simulated RBS spectra for (a) Al-40at.%Ta alloy, (b) Ta-22at.%Al alloy anodized at 5 mA/cm^2, to 150 V, in 0.01 M ammonium pentaborate electrolyte at 293 K. A thin outer alumina layer and an inner layer comprising units of Ta_2O_5 and Al_2O_3 are formed following anodizing of the alloy

Table 1 RBS-derived compositional data of the inner layer of the anodic oxide films formed on magnetron-sputtered tantalum-aluminum alloys

S.no.	Sample code	Composition derived from RBS, at.% Al	Ta	O	Density, g/cm^3	Ta_2O_5/Al_2O_3	Sputtering rate, q, g/m^2 s
1	T5AL1	5.62	26.03	68.35	7.35	6.12	0.82
2	T11A4	3.49	21.09	75.42	8.15	10.47	…
3	T23A2	8.24	23.04	68.72	7.02	3.85	0.84
4	T20AL	17	18.94	64.06	5.94	1.35	0.41
5	T10AL	8.95	16.73	74.32	6.93	3.47	0.81
6	A55T2	15.62	14.45	69.93	6.11	1.56	0.46
7	T30AL	16.10	11.95	71.95	6.4	2.04	0.37
8	TAO6	…	28.57	71.43	8.039	…	1.13

Table 2 RBS-derived composition of the magnetron-sputtered Ta-Al alloys

S.no.	Sample code	Composition derived from int./time rf-GDOES depth profile, c, at.% Al	Ta	Density, g/cm^3	Sputtering rate, q, g/m^2 s
1	T5AL1	24	76	15.92	2.18
2	T11A4	22	78	15.08	…
3	T23A2	27.5	72.5	15.86	2.02
4	T20AL	45	55	14.91	0.87
5	T10AL	52	48	13.18	2.35
6	A55T2	60	40	14.06	2.44
7	T30AL	71	29	12.87	1.39
8	TAO6	…	100	16.60	2.32

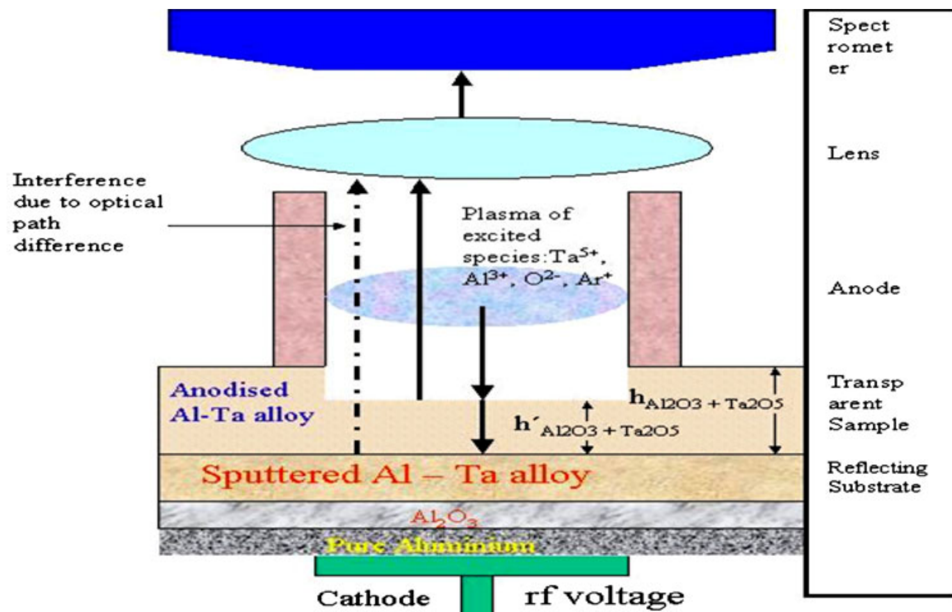

Fig. 3 Optical interference in the inner anodized Al_2O_3/Ta_2O_5 layer during rf-GDOES sputtering. The transparent layer is the anodized Al_2O_3/Ta_2O_5 layer, while the reflecting layer is the sputter-deposited Al-Ta alloy layer

(RBS), and Fig. 2(a) and (b) shows the measured and simulated RBS spectra for anodized Al-40at.%Ta and Ta-22at.%Al alloys. Simulations of the spectra, using the RUMP program, give the composition and thickness of the different layers of the film. Typical depth resolution is within the range 100-300 Å. All the results are presented in Tables 1 and 2.

3. Results and Discussions

3.1 Mechanism of Optical Interference in Anodized Ta-Al Alloys

The mechanism for optical interference in the inner layer (comprising units of Al_2O_3 and Ta_2O_5) of the anodized Ta-Al alloy film during rf-GDOES sputtering is illustrated in Fig. 3. During rf-GDOES sputtering, the sputtered aluminum, tantalum, and oxygen atoms from the inner film material enter the plasma and become excited by collision with energetic electrons or with excited "metastable" argon atoms. The sputtered atoms are de-excited by emitting photons of characteristic wavelength, thus returning to their fundamental energy level. De-excitation of the atoms produces the observed "glow."

The light emissions are scattered in all directions. However, only the light portion reflected vertically onto the surface being sputtered experiences the double reflection that leads to the optical interference effect. As illustrated in Fig. 3, one portion is reflected back from the sputtered surface, while the remainder passes through the sputtered sample thickness to be reflected back from the Ta-Al alloy interface. Both waves pass through the optical lens and interfere as a result of their phase difference, which is determined by the sample thickness. The changing sputtered surface results in the modulation of the intensity signal (or recorded photon signal at characteristic wavelength) as observed in the intensity/time depth profile. The measured or recorded signals at each characteristic wavelength measure the number of each type of atom sputtered from the sample layer.

The refractive index $n(\lambda)$ and the initial sample thickness, h_{layer}, may be determined from the relation (Ref 3)

$$2\,h_{layer} = k\lambda / n(\lambda) \qquad \text{(Eq 1)}$$

where λ and k represent the wavelength and the number of oscillations of the intensity signal, respectively.

The condition $n_{ar}^{+} < n_{layer} < n_{substrate}$ must be satisfied for optical interference to occur (Ref 3), i.e., the refractive index of the transparent layer must be greater than that of the discharge argon gas, but at the same time it must be less than that of the reflecting substrate for optical interference. Substituting the film thickness, determined from the electron micrographs, into Eq 1, the refractive indices for the various anodized Ta-Al alloys used in this work were found to lie between 1.4 and 2.4 (Table 3).

3.1.1 Mechanism of Optical Interference in the Inner (Al_2O_3) Layer. A relatively thin Al_2O_3 film also forms as a distinct layer at the surface of the film formed on Al-Ta alloys. This outer layer is represented in the rf-GDOES depth profile as the aluminum intensity signal, which has higher amplitude than the oscillation of the aluminum intensity signal in the inner layer of the film (Fig. 7). For the optical interference effect observed in the outer alumina layer, the transparent layer is the Al_2O_3 layer, while the reflecting or substrate layer is the inner layer. The conditions for optical interference previously discussed are satisfied since the refractive index of the transparent (Al_2O_3) layer is less than that of the reflecting (Al_2O_3/Ta_2O_5) substrate layer [determined to be between 1.7 and 2.4 (Table 3)] and less than that of the argon gas. During rf-GDOES sputtering through the Al_2O_3 layer, there is double reflection of the light waves at the characteristic aluminum

Table 3 Refractive indices of the inner layers (Ta_2O_5/Al_2O_3) of various anodized Al-Ta alloy films derived directly from their intensity/time rf-GDOES depth profile

S.no.	Sample code	Refractive index, n at λ_{Ta} (363 nm)	Refractive index, n at λ_{Al} (396 nm)	Ta_2O_5/Al_2O_3 ratio
1	TAO6	2.23	…	…
2	T5Al1	2.27	2.36	6.12
3	T20AL6	1.82	1.98	1.35
4	T10Al	1.84	2.0	3.47
5	A55T2	2.02	2.01	1.56
6	T23AL	2.08	2.27	3.85
7	T30AL1	1.75	1.73	2.04

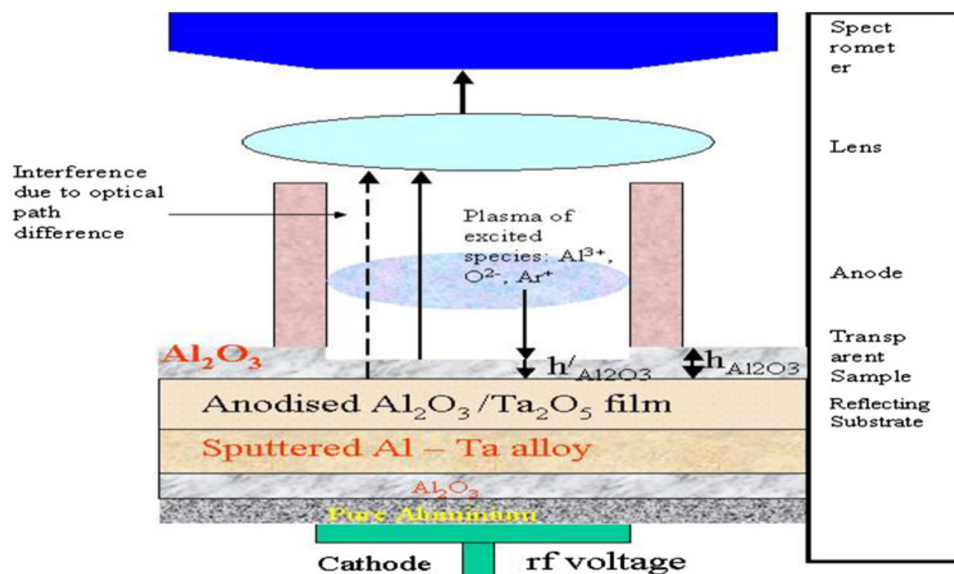

Fig. 4 First stage of the "serial" optical interference effect in the outer Al_2O_3 layer during rf-GDOES sputtering of anodized Al-Ta films. The transparent layer is the thin (10 nm) outer Al_2O_3 layer, while the reflecting layer is the inner anodized Al_2O_3/Ta_2O_5

wavelength. The first reflection occurs at the Al_2O_3 surface, which continually changes as it is sputtered, while the second reflection is at the Al_2O_3-Al_2O_3/Ta_2O_5 interface. This is illustrated schematically in Fig. 4.

3.1.2 Mechanism of Optical Interference in the Outer (Al_2O_3/Ta_2O_5) Layer. After the surface alumina layer has been completely removed by sputtering, optical interference also occurs in the inner layer during rf-GDOES sputtering through the anodized Al_2O_3/Ta_2O_5 layer. The Ta-Al alloy layer which lies below the transparent Al_2O_3/Ta_2O_5 layer now acts as the reflecting substrate. Thus, in the resultant rf-GDOES depth profile (for example Fig. 7), the oscillating aluminum intensity signal is observed across both layers of the anodized Ta-Al alloy. However, in the case of tantalum, the oscillating tantalum intensity signal is observed to fall to zero at the interface between the outer alumina layer and the inner Al_2O_3/Ta_2O_5 layer. This is further evidence of optical interference in the surface alumina layer.

Figure 7 shows that the amplitude of the oscillating aluminum peak corresponding to the outer Al_2O_3 layer is higher than the aluminum peaks in the Al_2O_3/Ta_2O_5 layer due to the higher content of aluminum (40 at.%) compared with the reduced aluminum content (15 at.%) in the Al_2O_3/Ta_2O_5 layer. The refractive indices of the anodized tantalum-aluminum alloy samples (29-100 at.% Ta) at the tantalum and aluminum wavelengths calculated using Eq 1 are displayed in Table 3. Figure 5 shows that the refractive index at the tantalum wavelength increases approximately linearly with the Ta_2O_5/Al_2O_3 ratio in the inner layer of the film.

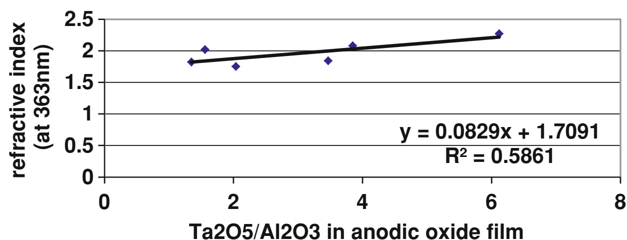

Fig. 5 Influence of Ta_2O_5/Al_2O_3 ratio on the refractive index of anodized Ta-Al alloys

3.2 Optical Interference in the Depth Profile of Anodized Al-40at.%Ta Alloy

Figure 6 shows a relatively thin anodic oxide film of 207 nm that is formed on the Al-40at.%Ta alloy layer. The absorption capacity for light waves is therefore reduced resulting in relatively large amplitudes of oscillation at the aluminum wavelength being observed in the depth profile shown in Fig. 7.

The electron micrograph of Fig. 6 also reveals two layers of the anodic oxide film consisting of an outer layer of relatively pure anodic alumina film of 10 nm thickness and an inner layer made up of an intimate mixture of Al_2O_3 and Ta_2O_5 units. As discussed earlier, there is optical interference in both layers during rf-GDOES sputtering. The depth profile (Fig. 7) thus reveals a high amplitude oscillation peak of the aluminum intensity in the anodic alumina layer and aluminum oscillation peaks of much smaller amplitudes in the inner layer of the film.

3.2.1 Determination of Composition Using the Optical Interference Effect. In Fig. 7, the peak in the outer film layer represents the 10-nm anodic Al_2O_3 layer. The second peak in the inner film layer consists of an intimate mixture of Al_2O_3 and Ta_2O_5 units. By stoichiometry, the aluminum content of the outer (Al_2O_3) layer is 40 at.%. The composition of the inner film layer (i.e., the region of the second peak) determined by RBS is 15.62 at.% Al, 14.41 at.% Ta, and 68.97 at.% O (sample A55T2 in Table 1). Intensity is directly proportional to concentration as given by the relationship $c_i\, q_n = f\,(I_i)$ (where c is concentration, q is sputtering rate, and I is the intensity). If composition across the film is uniform, then it is reasonable to assume that the sputtering rate across the inner layer of the Al_2O_3/Ta_2O_5 film is also constant. The slope of the oscillating profiles gives an indication of the extent of validity of the previous assumption (Ref 1). In accordance with the intensity/composition relationship, the composition of the inner film layer can be determined by equating the ratio of the intensity and composition in the outer Al_2O_3 layer with the ratio of the intensity and composition of the inner Al_2O_3/Ta_2O_5 film layer as follows:

Intensity of the aluminum peak in the inner Al_2O_3 layer/Intensity of the aluminum peak in the outer Al_2O_3/Ta_2O_5 layer = 44.5 V/16.8 V = 2.6.

Composition of aluminum in the outer Al_2O_3 layer/X (which represents the unknown composition of aluminum in the inner Al_2O_3/Ta_2O_5 layer) = 40 at.%/X at.%

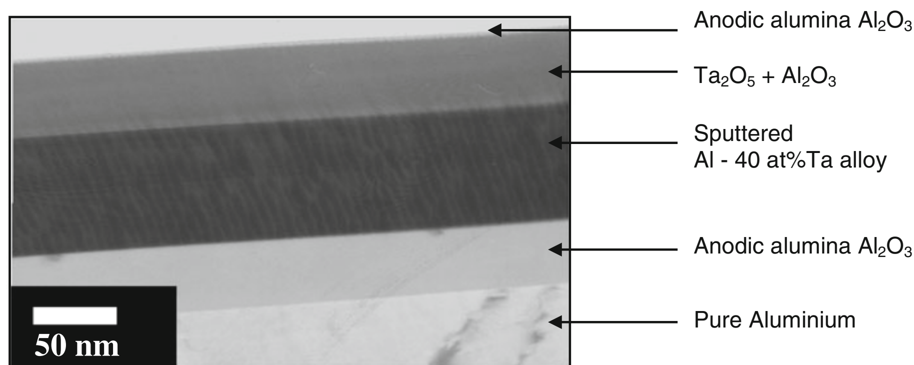

Fig. 6 Transmission electron micrograph of an ultramicrotomed section of the Al-40at.%Ta alloy and the anodic film formed at 5 mA/cm^2 to 250 V in 0.01 M ammonium pentaborate electrolyte at 293 K (A55T6)

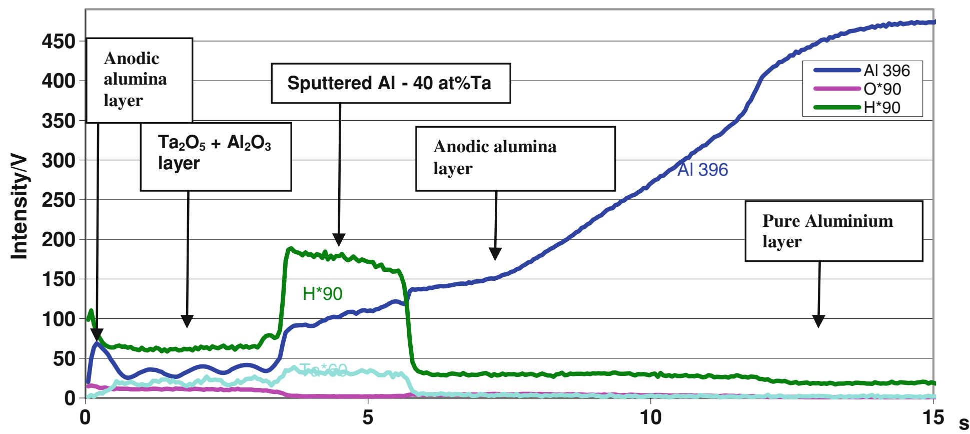

Fig. 7 Rf-GDOES depth profile of Al-40at.%Ta alloy anodized at 5 mA/cm^2 to 250 V in 0.01 M ammonium pentaborate electrolyte at 293 K. The higher intensity of the Al peak near the surface is due to optical interference within the outer anodic Al_2O_3 layer

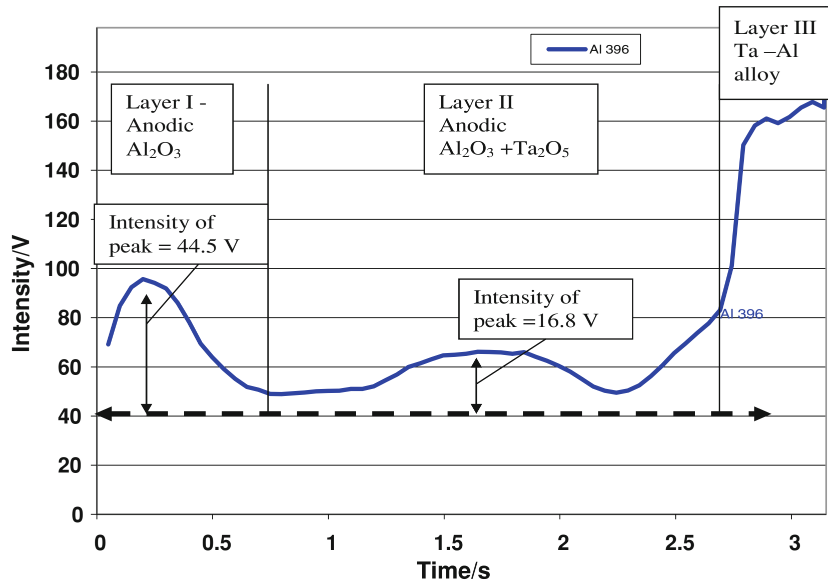

Fig. 8 Depth profile of anodized Al-40at.%Ta alloy showing uniform oscillation of the Al intensity signal through the film. The first oscillating peak is due to optical interference in the outer alumina layer. The optical interference effect permits determination of the composition of the inner layer film

Therefore, by equating the two parts, X which is the composition of aluminum in the Al_2O_3/Ta_2O_5 layer is determined to be 15.38 at.% (i.e., 40 at.%/2.6). The value obtained is in good agreement with the value of 15.62 at.% determined as the composition of aluminum in the inner layer by RBS (sample A55T2 in Table 1). Therefore, the optical interference effect permits determination of the composition of the inner layer of the anodic film from the intensity/time depth profile.

The aluminum intensity is observed to oscillate relatively uniformly across the film (Fig. 8). This indicates that the Al_2O_3 is uniformly distributed within the film matrix. Conversely, the oscillating tantalum intensity is observed to follow an upward slope toward the interface (Fig. 7). This trend can be explained by the non-uniform content of Ta_2O_5 across the film. The reason for the non-uniform composition is due to the slower migration rate of the Ta^{5+} ion compared with that of the Al^{3+} ion during film formation (Ref 24).

3.3 Optical Interference in the Depth Profile of Anodized Al-48at.%Ta Alloy

The depth profile of the film grown on Al-48at.%Al alloy (Fig. 9) shows four oscillation peaks of the tantalum intensity signal and 3 peaks of the aluminum signal in the anodic oxide film. No oscillation of the hydrogen signal is observed in the depth profile due to its absorption by the relatively thick film (425 nm). The aluminum peak in the outer Al_2O_3 layer of the film and the other aluminum peaks in the inner Al_2O_3/Ta_2O_5 layer oscillate uniformly across the film, although a slight slope of the aluminum peaks in the inner layer is evident. The tantalum signal is also observed to slope upward toward the film/alloy interface. As explained earlier, this may indicate variation of sputtering rate across the inner film layer, which may slightly interfere with the accuracy of the calculated composition given the assumption about constant sputtering

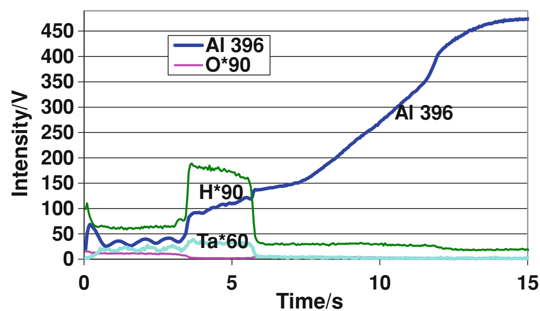

Fig. 9 Rf-GDOES depth profile of Al-48at.%Ta alloy anodized at 5 mA/cm^2 to 250 V in 0.01 M ammonium pentaborate electrolyte at 293 K. The oscillation of the tantalum and aluminum intensity signals observed in the transparent anodic Ta_2O_5/Al_2O_3 film layer is due to optical interference. The higher amplitude of the aluminum peak near the surface is due to optical interference within the pure anodic Al_2O_3 layer formed on the surface

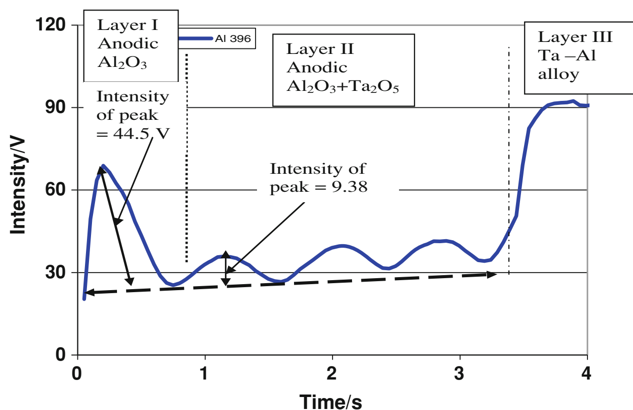

Fig. 10 Depth profile of anodized Al-48at.%Ta alloy showing the aluminum intensity oscillating uniformly through the Ta_2O_5/Al_2O_3 film

rate in the relation $c_i\ q_n = f(I_i)$. When the remaining thickness is completely sputtered, optical interference causes a maximum intensity to be reached at the alloy interface. This is represented in Fig. 10 by a dashed line, which also marks the end of the layer. From Eq 1, the refractive indices calculated for this anodized film at the tantalum and aluminum wavelengths are 1.84 and 2.0, respectively (Table 3).

3.3.1 Determination of Composition Using the Optical Interference Effect. Figure 10 shows that the amplitude of the aluminum peak in the Al_2O_3 layer is 4.6 times higher than those of the other aluminum peaks in the inner Ta_2O_5/Al_2O_3 layer. This is as a result of optical interference in the 5-nm-thick Al_2O_3 outer layer. The alumina layer in this film is thinner than the 10 nm obtained in the Al-40at.%Ta. Therefore, increased amplitude of oscillation resulting from the optical interference effect is expected. It can be shown again with this film that optical interference permits determination of the composition of the inner layer of the film (Fig. 10). The composition of aluminum in the outer Al_2O_3 layer (40 at.%) is higher than the composition of aluminum in the inner Al_2O_3/Ta_2O_5 layer (9.38 at.%). Thus, using the intensity/composition relationship given by $c_i\ q_n = f\ (I_i)$, the composition of the inner film layer is

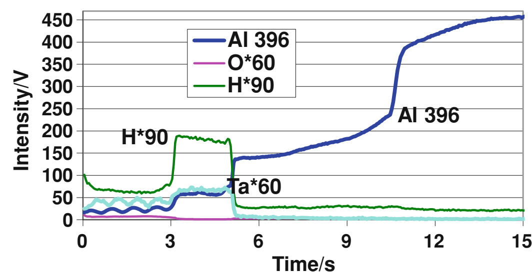

Fig. 11 Rf-GDOES depth profile of an anodic film grown on Ta-24%Al alloy to 250 V at 5 mA/cm^2 in 0.01 M ammonium pentaborate electrolyte at 293 K

determined by equating the ratio of the intensity and composition in the outer Al_2O_3 layer with the ratio of the intensity and composition of the inner Al_2O_3/Ta_2O_5 film layer as follows.

Intensity of the aluminum peak in the inner Al_2O_3 layer/ intensity of the aluminum peak in the outer Al_2O_3/Ta_2O_5 layer = 43.14 V/9.38 V = 4.6.

Composition of aluminum in the outer Al_2O_3 layer/X (which represents the unknown composition of aluminum in the inner Al_2O_3/Ta_2O_5 layer) = 40 at.%/X at.%.

Therefore, by equating the two parts, X (the composition of aluminum in the Al_2O_3/Ta_2O_5 layer) is 8.7 at.% (i.e., 40 at.%/ 4.6). The value obtained is in good agreement with the value of 8.95 at.% Al determined as the composition of aluminum in the inner layer by RBS (sample T10AL in Table 1).

3.4 Optical Interference in the Depth Profile of Anodized Ta-24%Al Alloy

Figure 11 shows the oscillation of the tantalum and aluminum intensities in the depth profile of anodized Ta-24%Al alloy. No intensity oscillation is observed at the hydrogen wavelength (122 nm) due to absorption by the film. Thick films have larger absorption edges than thin films. No oscillation of the oxygen (130 nm) intensities is observed, again due to absorption by the film. Usually, the optical interference effect is not observed for lines with wavelengths below 200 nm (Ref 1). As the proportion of Ta_2O_5 to Al_2O_3 increases, the refractive index, $n(\lambda)$, also increases (Fig. 5). Thus, the transparency of the film, characterized by its refractive index relative to that of the reflecting substrate, is largely governed by the effective tantala (Ta_2O_5) content. The proportion of Ta_2O_5 to Al_2O_3 in the inner Ta_2O_5/Al_2O_3 layer of the Ta-24%Al alloy is 6.12 (Table 3). Using Eq 1, the refractive indices calculated at the Ta and Al wavelengths are 2.27 and 2.36, respectively. Thickness data, h_{layer}, used for the calculation were obtained from the electron micrographs.

Oscillations at both wavelengths are observed to terminate at common maxima. This represents the last sputtered thickness before the alloy interface is reached. There is no appreciable oscillation lag at the film surface as oscillation is observed to start almost from the surface, although a short plasma stabilization time is implied. The oscillating aluminum and tantalum signals are observed to be relatively uniform across the film, which is thus compositionally uniform. The observed uniformity also indicates excellent depth resolution which may be inferred from the presentation of the oscillations. Usually, decreasing oscillation amplitude with depth implies light

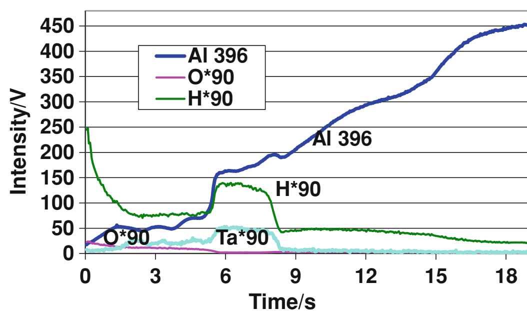

Fig. 12 Rf-GDOES depth profile of an anodic film formed Al-29at.%Ta alloy to 250 V at 5 mA/cm^2 in 0.01 M ammonium pentaborate electrolyte at 293 K

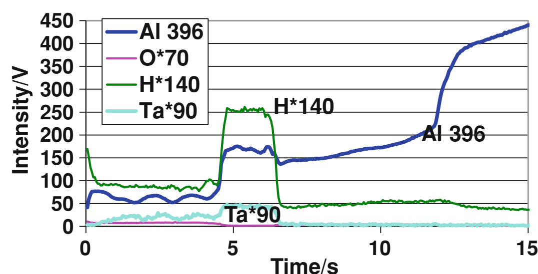

Fig. 13 Rf-GDOES depth profile of an anodic film grown on Ta-45%Al alloy to 250 V at 5 mA/cm^2 in 0.01 M ammonium pentaborate electrolyte at 293 K. The aluminum and tantalum intensity signals oscillate uniformly through the film, indicating uniform distribution of Al_2O_3 and Ta_2O_5 within the film

reflection from an increasingly uneven crater bottom and eventual superposition of light waves reflected from different depths, which is present in the depth profile as smaller amplitudes of oscillation. In the depth profile of this film, the amplitudes of oscillation are observed to be relatively uniform (Fig. 11). Thus, it may be inferred that the crater bottom is reasonably flat up to the interface, giving an excellent depth resolution. Due to progressive thinning of the sample thickness during sputtering, the amplitude of oscillation is observed to increase slightly with depth. This is explained by the fact that the smaller the film thickness, the smaller the amount of absorption of the waves, and hence the greater the amplitude of oscillation that is observed (Ref 2).

3.5 Optical Interference in the Depth Profile of Anodized Al-29at.%Ta Alloy

Figure 12 shows the oscillation of the intensities of the tantalum and aluminum signals in the intensity/time depth profile of the Al-29at.%Ta alloy film. Using Eq 1, the refractive indices $n(\lambda)$ at the tantalum and aluminum wavelengths (363 and 396 nm) were calculated to be 1.8 and 1.37, respectively. The thickness of the film, h_{layer}, was determined from the electron micrograph.

The depth profile intensities of both the tantalum and aluminum signals can be observed in Fig. 12 to terminate at the common maxima at the interface with the alloy. This satisfies optical theory as it represents the last film thickness sputtered before the alloy substrate is encountered. The changing slope of the oscillating aluminum signal near the interface with the alloy substrate corresponds with progressive degradation of depth resolution observed in the interface region (Fig. 12). The degradation of depth resolution is a result of the steep change in sputtering rate between the film (0.30 g/m^2 s) and the alloy (1.39 g/m^2 s). This represents a 466% increase in sputtering rate at the interface. The tantalum and aluminum signals in the film that is located further from the interface are, however, observed to oscillate relatively uniformly. Non-uniform oscillation due to degradation of depth resolution has been associated elsewhere (Ref 3) with errors in the calculated thickness. Close to the surface, the tantalum signal is observed to drop to zero after background subtraction (Fig. 12). A very thin alumina layer is formed in the outer layer, which is confirmed by electron microscopy. No optical interference is observed in this layer because the film thickness is too small (2 nm) compared with the wavelength of aluminum (396 nm).

The oscillations of the aluminum and tantalum signals (Fig. 12) are observed to have equal amplitudes. Thus, each oscillation peak represents a fraction of the total film thickness. In this case, each oscillation peak of the aluminum signal represents approximately 114.3 nm. Consequently, the thickness of the film can be rapidly estimated by multiplying by the number of oscillation peaks in the depth profile exhibiting optical interference. However, when the oscillation peaks have unequal amplitudes, there is a reduction in the accuracy of the film thickness determined.

3.6 Optical Interference in the Depth Profile of Anodized Ta-45%Al Alloy

Figure 13 show three oscillation peaks for the tantalum and aluminum signals in the depth profile of the anodized Ta-45%Al alloy film. For the aluminum signals, however, optical interference in the outer alumina layer reveals an aluminum peak, which has a higher intensity than the two peaks in the inner Ta_2O_5/Al_2O_3 layer. All three tantalum peaks are located in the inner Ta_2O_5/Al_2O_3 layer. The tantalum intensity in the outer alumina layer falls to zero in this layer. Thus, it can be confirmed that pure anodic alumina is formed on the surface of the film. No oscillation of the hydrogen signal is observed due to absorption by the film (330 nm). Figure 13 shows that the aluminum signal oscillates uniformly across the film, while a slight slope is observed for the tantalum signal near the interface; at the film/alloy interface, both signals terminate at the common maxima, thus validating optical theory. Refractive indices for the film calculated from Eq 1 gave values of 1.87 and 2.0 at the Ta and Al wavelengths, respectively (sample T20Al6 in Table 3).

3.7 Procedure for Direct Quantification of Depth

The method for calculating the thickness of the transparent layer of anodic oxide films exhibiting optical interference, using Eq 1, has been demonstrated for several films formed on Al-Ta alloys. Knowledge of the refractive index of the transparent media is required for the calculation. Approximate values may be obtained from the literature sources for standard materials. However, for non-conventional materials such as anodic oxide films, the optical properties may vary depending on the conditions of formation. Thus, the required value of the refractive index may be obtained to a reasonable accuracy by calibrating the refractive index (determined from the film

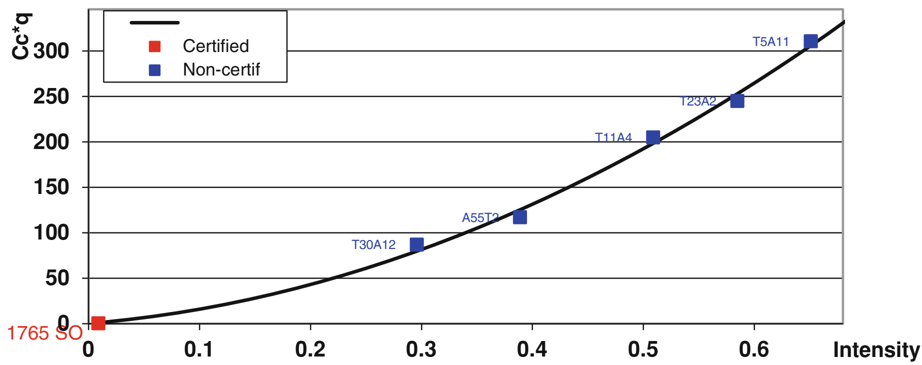

Fig. 14 Second-order calibration curve for tantalum 363 nm

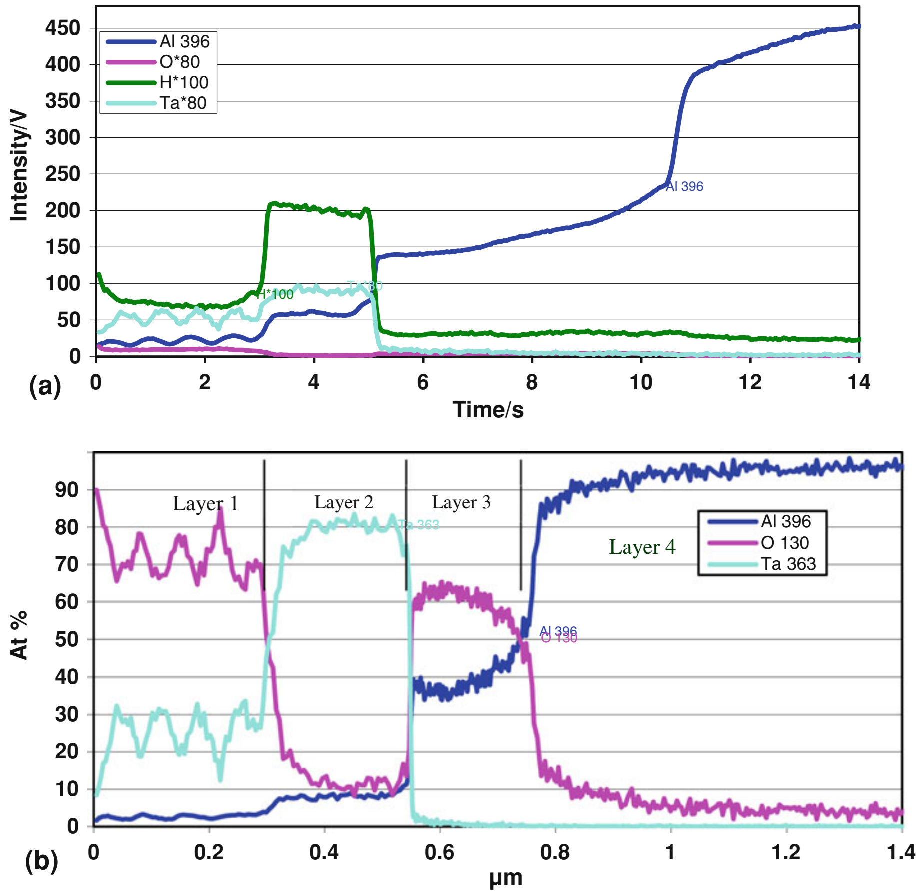

Fig. 15 (a) Qualitative (int vs. time), (b) quantitative (at.% vs. µm) rf-GDOES depth profiles for Ta-24 at.% Al alloy anodized at 5 mA/cm^2 to 250 V in 0.01 M ammonium pentaborate electrolyte at 293 K. Layer 1 represents anodic Ta_2O_5 + Al_2O_3, layer 2 is Ta-Al alloy, layer 3 is anodic alumina (Al_2O_3), and layer 4 is superpure aluminum substrate

thickness which is in turn determined from electron micrographs) with the concentrations of the depth profile elements (determined by RBS), which have oscillating signals. A procedure for quantification of depth directly from the rf-GDOES intensity/time depth profile for elements with oscillating signals (i.e., due to the optical interference effect) is proposed below using films formed on magnetron-sputtered Al-Ta alloys as the example.

1. Grow the anodic oxide film from Al-Ta alloys with known concentrations of aluminum and tantalum. Usually, this may be achieved by magnetron sputtering from the respective targets followed by anodic oxidation of the sputtered alloy.
2. Prepare plots of tantalum concentration (at.% Ta) and aluminum concentration in the Al-Ta alloy versus tantalum concentration (at.% Ta) and aluminum concentration (at.% Ta) in the anodic film. In Fig. 6, these plots are shown to be linear and can be used to determine the concentrations of both tantalum and aluminum in the anodic oxide film from the known concentration of the Al-Ta alloy from which it was grown. The same anodizing conditions, especially current density, should be used for

both the calibrating Al-Ta alloys and the validating or unknown Al-Ta alloy. A current density of 5 mA/cm^2 was used in this study.
3. Use the values determined in 2 above to determine the refractive indices at the tantalum and aluminum wavelengths from the plot of the Ta_2O_5/Al_2O_3 ratio versus refractive index (Fig. 5).
4. Substitute the value of the refractive index obtained into Eq 1 to calculate the required film thickness.
5. The film thickness value determined may then be used in the quantification software for conversion of the time scale to depth scale.

3.8 Rf-GDOES Depth Profile Quantification

In order to prepare calibration standards for quantification of the rf-GDOES depth profiles, for each of the anodized alloys, all the atoms in each layer were summed and the percentage of each element calculated. The RBS-derived compositions are presented in Ref 24. The resultant concentrations were then used in conjunction with their Rf-GDOES intensities to prepare calibration curves for Ta, Al, and O. The second-order calibration curve for Tantalum is shown in Fig. 14. These were then used for quantification of the qualitative rf-GDOES depth profiles of the anodized Al-Ta alloy films as shown in Fig. 15. A more complete description of quantification process is presented elsewhere (Ref 24). The quantitative depth profile permits exploration of the composition/concentration and distribution of species within the multilayer films with depth, with an excellent depth resolution of less than 1 nm, indicating minimal atomic mixing associated with film sputtering. Accuracy of the determined composition is excellent at ±0.2 for the anodic alumina film compared with the composition determined by RBS. For depth, there is good agreement of ±5.5 for anodic alumina due to the precisely known density and ±9 for the anodized Ta-Al alloy layer, consistent with the accuracy of the calculated density. The large error of ±15.5 for the Ta-Al alloy layer is in correlation with the uncertainty in the calculated density. These error margins for the depth were estimated by comparison with the corresponding layer thickness determined from the transmission electron micrograph.

4. General Conclusions

Oscillation of Ta and Al signals is observed in rf-GDOES depth profiles of a wide range of anodized Ta-Al alloys. The calculated refractive indices of Ta and Al in the anodized Ta-Al alloy layer are 1.75-2.23 and 1.73-2.36, respectively, which compare very well with values obtained by other workers. These values were obtained by substituting the TEM-derived layer thickness into the relationship $2\ h_{layer} = k\ \lambda/n(\lambda)$.

The use of intensity/time rf-GDOES depth profiles to determine the composition of anodic oxide layers exhibiting optical interference is demonstrated for the first time. For anodized Al-40at.%Ta alloy, the determined composition (15.38 at.% Al) was in good agreement with the composition determined by RBS (15.62 at.%). The composition was obtained using the relationship $c_i\ q_n = f(I_i)$ and by comparing the known depth profile intensity and composition (40 at.%) of Al in the outer anodic alumina layer with the known intensity and unknown composition in the anodized layer. For the anodized Al-48at.%Ta alloy, the determined composition (8.70 at.% Al) was also in excellent agreement with the RBS-determined composition of 8.95 at.%.

A procedure is proposed for determination of film thickness directly from intensity/time rf-GDOES depth profiles. The thickness is determined by substituting refractive index (obtained from the linear calibration plot of intensity versus Ta_2O_5/Al_2O_3) into the relationship $2\ h_{layer} = k\ \lambda/n(\lambda)$. A potential application is possible inclusion as a feature in current rf-GDOES quantification software.

The conversion of intensity/time rf-GDOES depth profiles to composition/depth is presented for anodized Ta-24at.%Al alloy. The accuracy of the determined composition and depth of the anodic alumina layer is excellent. However, the accuracy of the determined depth is ±9 nm for the anodized Ta-Al alloy layer and ±15 nm for the Ta-Al alloy layer, correlating with the accuracy of the calculated density.

Acknowledgments

The author is grateful for the support for this work by the University of Manchester (Corrosion and Protection Centre), formerly University of Manchester Institute of Science and Technology, and Jobin Yvon Horiba, France. Special thanks to Professor G. E. Thompson for supervising and facilitating the critical resources required for the study, Prof. P. Skeldon for his assistance with RBS and critical discussion of this work, and Mr. P. Chapon of Jobin Yvon Horiba, France, for providing access to the rf-GDOES instrument and also his insight into the GD industry.

Open Access

This article is distributed under the terms of the Creative Commons Attribution License which permits any use, distribution, and reproduction in any medium, provided the original author(s) and the source are credited.

References

1. R. Dorka, R. Kunze, and V. Hoffman, Investigation of SiO_2 Layers by Glow Discharge Optical Emission Spectroscopy Including Layer Thickness Determination by an Optical Interference Effect, *J. Anal. Atomic Spectrom.*, 2000, **15**, p 873–876
2. S. Kimura and Y. Mitsui, Effect of Optical Interference on Borophosphosilicate Glass Profiles Obtained with a Glow Discharge Optical Emission Spectrometer, *Appl. Spectrosc.*, 2001, **55**(3), p 292–296
3. V. Hoffman, R. Kurt, K. Kammer, R. Thielsch, T. Wirth, and U. Beck, Interference Phenomena at Transparent Layers in Glow Discharge Optical Emission Spectrometry, *Appl. Spectrosc.*, 1999, **53**(8), p 987–990
4. M. Forest and P. Cheetham, Ta for the Future, *Mater. World*, 2002, **10**(10), p 14
5. Organic Electronics, Google books, http://books.google.co.uk/books
6. Z. Geretovszky, T. Szorenyi, P. Stoquert, and I.W. Boyd, Correlation of Compositional and Structural Changes During Pulsed Laser Deposition of Tantalum Oxide Films, *Thin Solid Films*, 2004, **453-454**, p 245–250
7. S. Ezhilvalavan and T. Tseng, Preparation and Properties of Tantalum Pentoxide (Ta_2O_5) Thin Films for Ultra Large Scale Integrated Circuits (ULSIs) Application—A Review, *J. Mater. Sci. Mater. Electron.*, 1999, **10**(1), p 9–31
8. H. Yoshino, T. Ihara, S. Yamanaka, and T. Igarashi, Tantalum Oxide Thin-Film Capacitor Suitable for Being Incorporated into an Integrated Circuit Package, *Sixth IEEE/CHMT International Japan IEMT Symposium*, 26-28 Apr 1989

9. J. Adams and D. Kramer, A Study of the Oxidation of Tantalum Nitride by Ellipsometry and Auger Electron Spectroscopy, *Surf. Sci.*, 1976, **56**, p 482–487
10. C.L. Au, W.A. Anderson, D.A. Schmitz, J.C. Flassayer, and F.M. Collins, Stability of Tantalum Nitride Thin Film Resistors, *J. Mater. Res.*, 1990, **5**, p 1224–1232
11. P.C. Joshi, M.W. Cole, C.W. Hubbard, E. Ngo, Al Doped Ta_2O_5 Thin Films for Microelectronic Applications, MRS Proc. 2000, **654**, p AA7.10.1
12. L.J.D. Zekovic and V.V. Urosevic, New Investigations of the Interference Effect in Electroluminescence of Anodic Films on Aluminium, *Thin Solid Films*, 1981, **86**(4), p 347–350
13. S. Jiaming, Z. Guozhu, F. Xiwu, F. Guozhu, and Z. Chenwei, Electroluminescence from ITO/SiO_2/Ta_2O_5/Al Multiple-Layer Structure Excited by Hot Electrons, *J. Non-Cryst. Solids*, 1997, **212**(2-3), p 192–197
14. G.F. Pastore, Transmission Interference Spectrometric Determination of the Thickness and Refractive Index of Barrier Films Formed Anodically on Aluminium, *Thin Solid Films*, 1985, **123**(1), p 9–17
15. L.J. Zekovic, V.V. Urosevic, and B. Jovanic, Determination of Anodic Oxide Film Thickness by a Luminescence Method, *Appl. Surf. Sci.*, 1982, **11-12**, p. 90–99
16. J.K. Solberg, Double-Refraction Theory Applied to Anodic Films on Aluminium, *Metallography*, 1986, **19**(2), p 197–207
17. L. Zhao, J. Wang, Y. Li, C. Wang, F. Zhou, and W. Liu, Anodic Aluminum Oxide Films Formed in Mixed Electrolytes of Oxalic and Sulfuric Acid and Their Optical Constants, *Physica B*, 2010, **405**(1), p 456–460
18. J.D. Klein, A. Yen, and S.F. Cogan, Determining Thin Film Properties by Fitting Optical Transmittance, *Journal of Applied Physics*, 1990, **68**(4), p 1825–1830
19. A.A. Barybin, A.V. Mezenov, and V.I. Shapovalov, Determining the Optical Constants of Thin Oxide Films, *J. Opt. Technol.*, 2006, **73**(8), p 548–554
20. F. Mitsugi, A. Matsuoka, Y. Umeda, and T. Ikegami, Development of Thickness Measurement Program for Transparent Conducting Oxide Thin Films, *Thin Solid Films*, 2010, **518**(22), p 6330–6333
21. R. Chiu and P. Chang, Thickness Dependence of Refractive Index for Anodic Aluminium Oxide Films, *J. Mater. Sci. Lett.*, 1997, **16**, p 174–178
22. S. Van Gils, C.A. Melendres, and H. Terryn, Quantitative Chemical Composition of Thin Films with Infrared Spectroscopic Ellipsometry: Application to Hydrated Oxide Films on Aluminium, *Surf. Interface Anal.*, 2003, **35**(4), p 387–394
23. C.A. Melendres, S. Van Gils, and H. Terryn, Toward a Quantitative Description of the Anodic Oxide Films on Aluminium, *Electrochem. Commun.*, 2001, **3**(12), p 737–741
24. D. Ifezue, "Quantitative Analysis of Anodic Oxide Films by Radio Frequency Glow Discharge Optical Emission Spectroscopy (Rf-GDOES)," PhD Thesis, University of Manchester Institute of Science and Technology, 2004
25. Presentations by P. Chapon, Glow Discharge Technical Support, Version 1.1, Jobin Yvon Horiba, January 2003